Experimental proof of a thermal system for cooling and storage applications employing cacl2/silica gel composite adsorbent

Energy Conversion and Management 341 (2025) 120072

Contents lists available at ScienceDirect

Energy Conversion and Management

journal homepage: www.elsevier.com/locate/enconman

Experimental proof of a thermal system for cooling and storage applications employing cacl$_2$/silica gel composite adsorbent☆

Valeria Palomba [a,*], Andrea Frazzica [a], Vincenza Brancato [a], Antonino Bonanno [a], Yannan Zhang [a,b], Matteo Calò [c], Gabriele Penello [d], Gabriel Yarce [d], Walter Mittelbach [d]

[a] National Research Council of Italy – Institute for Advanced Energy Technologies (CNR-ITAE), Salita S.Lucia sopra Contesse 5, 98126 Messina, Italy
[b] School of Materials and Energy, Guangdong University of Technology, Guangzhou 510006, China
[c] Politecnico di Torino, Department of Energy. Turin 10129, Italy
[d] Sorption Technologies GmbH. Freiburg 79098, Germany

ARTICLE INFO

Keywords:
Adsorption
Chemisorption
Selective water sorbents
Thermochemical storage
Adsorption chiller

ABSTRACT

Sorption systems have been widely studied for cooling applications and as thermochemical energy storage devices for provision of heating and cooling, according to seasonal requirements. In the latest years, several researchers worked on the development of composite adsorbent materials for such kind of applications, but the vast majority of work is limited to material scale or small-scale devices. In the present paper, the experimental results on a lab-scale prototype of a sorption system are presented. Its main innovative features are the use of a composite made with silica gel and calcium chloride ($CaCl_2$) (25 % wt. of salt inside the silica matrix) along with a patented method for evaporation/condensation, which makes usage of a porous structure directly inserted in the vacuum chamber with the heat exchanger and the storage material. Experimental tests were carried out considering both the possibility of using the system as a chiller and as a thermochemical storage. In chiller operation, average powers up to 6 kW were measured, and thermal energy storage capacity of 14 MJ (cooling storage operation) and 19 MJ (heat storage operation) were measured, thus indicating that the application of composite materials in large scale systems for real-world application is feasible and efficient.

1. Introduction

The use of sorption systems for mid to long-term storage applications and for waste heat recovery is gaining interest, not only for the residential areas but also in combination with district heating and cooling (DHC). At the same time, the energy system of the future is intended to accommodate a larger share of renewables inside the grids (thermal and electric), which requires suitable storage systems for peak shaving and load shifting [1].

Sorption systems allows to answer to such challenges, thanks to their high flexibility (they can be operated for heating and cooling purposes), virtually lossless storage operation and possibility of being installed also in residential areas or in buildings (differently from underground storage or aquifer storage). The main challenges that sorption technology has to face are: possibility of using non-toxic materials and refrigerants, that would hinder installation in buildings; the need for high energy density and power and a regeneration temperature compatible with low-grade heat and waste heat recovery (<80 °C) [2].

In order to tackle these challenges, the vast majority of studies in this field have focused on the development and characterization of materials [3–5]. Among the various classes of materials available for sorption systems, salt hydrates were identified as the most promising ones, both for heating/cooling applications, for thermal storage and for desalination systems. Examples of salts that are considered as promising candidates for low-temperature heat storage are calcium chloride ($CaCl_2$), magnesium sulfate ($MgSO_4$) [6], magnesium chloride ($MgCl_2$) [7], aluminium sulfate (Al_2SO_4), sodium sulfide (Na_2S) and strontium chloride ($SrCl_2$) [8,9]. LiCl and $CaCl_2$ are considered also promising candidates for the use in thermal desalination systems [10]. At material level the research focused on two main aspects: improving the thermal stability of the materials and improving the dynamics and reversibility of the reactions involving the storage process with salt hydrates[11]. One of the most common methods to achieve these goals is to embed the salt hydrates in porous matrices, such as zeolites, mesoporous silica gels and even MOFs [12].

☆ This article is part of a special issue entitled: 'ECOS2024_ECM' published in Energy Conversion and Management.

* Corresponding author.
E-mail addresses: valeria.palomba@cnr.it (V. Palomba), matteo.calo@polito.it (M. Calò).

https://doi.org/10.1016/j.enconman.2025.120072

Available online 16 June 2025

Nomenclature

A	area, m^2
cp	specific heat capacity, kJ/(kg K)
H	specific enthalpy, kJ/kg
$\dot{m}$	mass flow rate, kg/s
p	pressure, bar
Q	Energy, kJ
$\dot{Q}$	Thermal power, kW
U	Heat transfer Coefficient, kW/(K m^2)
T	temperature, °C
t	time, s
ad	adsorption
cd	condenser
cond	condensation
de	desorption
eq	equilibrium
ev	evaporator
eva	evaporation
in	inlet
out	outlet
ref	refrigerant
sat	saturation

Abbreviations

COP,th	thermal Coefficient of Performance
D-A	Dubinin-Ashtakov
HT	High Temperature, °C
HTF	Heat Transfer Fluid
LMTD	Logarithmic Mean Temperature Difference
LT	Low Temperature, °C
MT	Medium Temperature, °C
SCP	Specific Cooling Power, kW/kg
SG	Silica Gel

Despite these efforts, several challenges remain. Issues related to the scalability of these materials, long-term cycling degradation, and the complexity of system integration are still being addressed. Indeed, only a few examples of systems employing salt hydrates and composites realized with salt hydrates were scaled up to lab systems [13]. Moreover, the manufacturing of large scale adsorption chillers was demonstrated to be still not sustainable from the economic point of view [14]. In this regard, the design of the reactors proved to be another key factor. However, as highlighted in a recent review [3], there have been no substantial improvement in the design of heat exchangers and reactors in the last decade, with only some exceptions related to the application of numerical methods such as topology optimization for the realization of thermochemical storage systems [15].

In this context, the current paper follows the overall design, manufacturing and testing of a prototype of adsorption chiller, which employs, for the first time in the literature, a large amount of composite material realized with mesoporous silica gel impregnated with calcium chloride (i.e. 75 kg). Moreover, the prototype is based on a novel design of adsorption systems, which has never been presented in the literature. The main innovation consists in the use of a porous structure in the adsorption/desorption chamber through which the refrigerant is flown in liquid form, whereas an external plate heat exchanger is used for the evaporation/condensation. The prototype was tested both as a chiller and as a thermal energy storage system. The selection of material, its preparation and characterization are discussed in section 2 The novel design and operating principle are presented in section 3, alongside with the manufacturing details of the prototype. Experimental results are discussed in section 4 and are extensively discussed in section 5 and 6, where the main novelties and findings in the experimental testing of the prototype are compared to the most recent prototypes of sorption chillers and thermal storage in the literature.

2. Materials

2.1. Material selection and preparation

The selected material is a composite made with 25 % wt. calcium chloride ($CaCl_2$) supported on mesoporous silica gel (SG), belonging to the class of "salt in porous matrix" sorbents. $CaCl_2$-based composites have been widely tested in the last years for thermochemical energy storage [13,16,17], showing excellent energy storage capacity. Moreover, the application of this class of materials has also shown promising potential in desalination cum cooling applications [10].

Dry impregnation method at atmosphere pressure was utilized to prepare the composite sorbent, which consists of the following steps [18]:

1. Drying of the matrix and the salt in oven at 150 °C for 8 h.
2. Solution preparation by mixing distilled water with the salt. The amount of water needed is calculated based on the pore volume of the matrix and the overall mass of salt to be embedded inside the matrix itself.
3. Dropping of the solution onto the matrix. It was verified that, in order to have a proper distribution of the salt inside the matrix it is necessary to continuously mix the material under preparation.
4. Drying of the composite for 8 h in oven.

The material for the prototype was prepared in large batches (kg scale) at CNR. In this case a large plastic mixer was used for the preparation of the salt solution and the dropping of the solution was achieved by continuously rotating the adsorbent material inside the mixer while spraying the solution at regular intervals by means of a stainless steel shower head.

The main physical properties of the mesoporous silica gel are presented in Table 1, whereas for the calcium chloride they are presented in Table 2.

2.2. Material characterization

Water adsorption isotherms/isobars of the manufactured composite material were measured with a thermo-gravimetric technique based on the use of an automated vapor sorption analyzer (DVS Vacuum, Surface Measurement Systems Ltd.). The core of the instrument is a CAHN microbalance with the following features: sample mass 5——1000 mg, mass change: ±150 mg, resolution (precision): 0.1 μg. The procedure used to carry out the tests consists of a first degas phase of the sample at high temperatures (150 °C) and high vacuum (10–4 kPa) for 5 h in order to evacuate and regenerate the sample. The dry mass in obtained once it is completely degassed, then the measure of the equilibrium data, in isobar or in isotherm condition starts.

Fig. 1 shows the equilibrium curves of the SG-25 % $CaCl_2$ composite.

Table 1
Properties of mesoporous silica gel used for the composite.

Material	Particle size (mm)	Surface area (m2/g)	Nominal Pore Volume (cm3/g)	Pore size (nm)	Price (€/100 kg)
Mesoporous silica gel	0.3 – 0.8	≈390	0.95	8 – 12	500

Table 2
Properties of calcium chloride.

SALT	CAS	molecular weight	Density (g/cm3)	Purity	Seller	Price (€/kg)
$CaCl_2$	10043–52-4	110.98	2.15	≥ 99 %	Sigma Aldrich	≈ 5[1]

[1] The price is based on quotations asked by the industrial partners among the authors of the paper for large batches (>100 kg) in the EU.

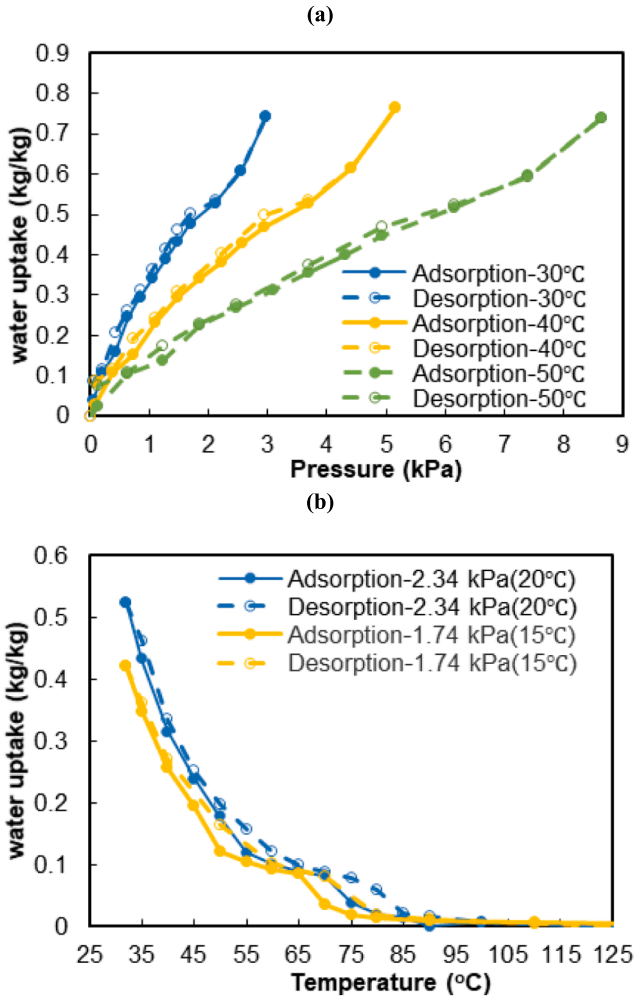

Fig. 1. (a) Sorption isotherms, (b) sorption isobars for the SG-25% $CaCl^2$ composites.

Both isotherms (Fig. 1a) and isobars (Fig. 1b) were measured and the adsorption and desorption curves are reported, in order to verify if there is any hysteresis. The amount of water uptake increases with the increased vapor pressure and decreased adsorption temperature. The maximum water uptake is 0.75 g/g. A plateau appears on the sorption isobar approximately for a water uptake of around 0.1 g/g, which is caused by the phenomena of hydration reaction of the salt contained in the composite. Afterwards, an almost linear water uptake increase is highlighted, due to the water absorption in the salt solution formed inside the pores of the matrix. The presence of hysteresis, which is not remarkable in the isotherms, is instead clearly visible in the isobars from Fig. 1b.

Moreover, the cycled water uptake, sorption heat and sorption enthalpy under different operating conditions for heating and cooling applications were measured using a modified Setaram TG/DSC apparatus capable of operating under saturated vapor conditions. For heating applications, two operating temperature boundaries were measured, corresponding to the availability of heat sources for regeneration at 70 °C and 90 °C, whereas for cooling application, the tested conditions correspond to warm temperature climates with heat rejection in ambient air. The results are summarized in Table 3. The range of the obtained sorption enthalpy is 2530–2633 kJ/kg H_2O under various operating conditions, with a slight increase for increasing desorption temperature.

The possible degradation of the composite was evaluated. To this aim, tests in conditions similar to the large-scale ones were carried out in a lab-scale prototype at CNR (nominal heat storage capacity of 2 kWh). After 100 cycles, the material was removed from the heat exchanger and tested in the DVS apparatus. The comparison between the two isobars of the fresh and cycled material is shown in Fig. 2: as it is possible to notice there is basically no deviation in the adsorption capacity, thus indicating no degradation of the material.

3. Prototype design and development

3.1. Operating principle

The operating principle of the tested prototype is schematically presented in Fig. 3 and differs from the typical configuration of an adsorption heat conversion machines. Indeed, in this concept, the adsorption module consists of the heat exchanger with the adsorbent material (i.e. the adsorber) and a volume of the adsorption chamber filled with a porous structure. During the desorption phase, the adsorber module is heated up by the external heating source and the desorbed water is directly condensed over the porous structure integrated inside the adsorber chamber. Indeed, the refrigerant (i.e. water) is contained in a separated vacuum vessel in its liquid state in equilibrium with its vapor. During the discharging phase, the liquid water is firstly pumped through an external plate heat exchanger (HEX), connected to the heat rejection unit, and then dropped onto the porous structure contained inside the adsorber chamber. In this way, the desorbed water is condensed directly on the porous structure and the heat of condensation is taken over by the water flowing down by gravity. The exiting hotter water flows back to the vacuum tank at the bottom.

During the adsorption process, the adsorber module is connected to the evaporator tank, that is, in turn, connected to an external plate HEX to exchange heat with the chilled water heat transfer fluid (HTF) circuit. The liquid refrigerant is dropped onto the porous structure, where direct evaporation occurs and it is then adsorbed by the material. Accordingly, the water exiting from the bottom of the adsorber chamber is colder thus producing the cooling effect. In this concept, the overall heat transfer efficiency is enhanced and it is possible to make use of compact plate HEXs instead of large evaporator and condenser. Moreover, the refrigerant is distributed inside the system in its liquid phase, instead of vapor one, reducing the size of internal piping and valves, thanks to the much higher density of liquid water compared to the vapor phase. This is beneficial also from the cost perspective point of view. The refrigerant flow is achieved by means of side channel pumps, which can also work in the operating conditions of a closed adsorption machine, i.e. under liquid–vapour equilibrium.

Table 3
Summary of TG/DSC results of SG-25% $CaCl_2$ composites.

Application $T_{de}(T_{cond})$/ $T_{ad}(T_{eva})$	Heating 70(20)/40(20) °C	90(20)/40(20) °C	Cooling 70(20)/35(15) °C
w [g/g]	0.18	0.23	0.21
Q_{ad} [kJ/$kg_{material}$]	471.02	570.90 ± 28.5	536.18 ± 26.8
ΔH_{ad} [kJ/kg_{water}]	2576.00	2633.14 ± 131.6	2530.95 ± 126.5

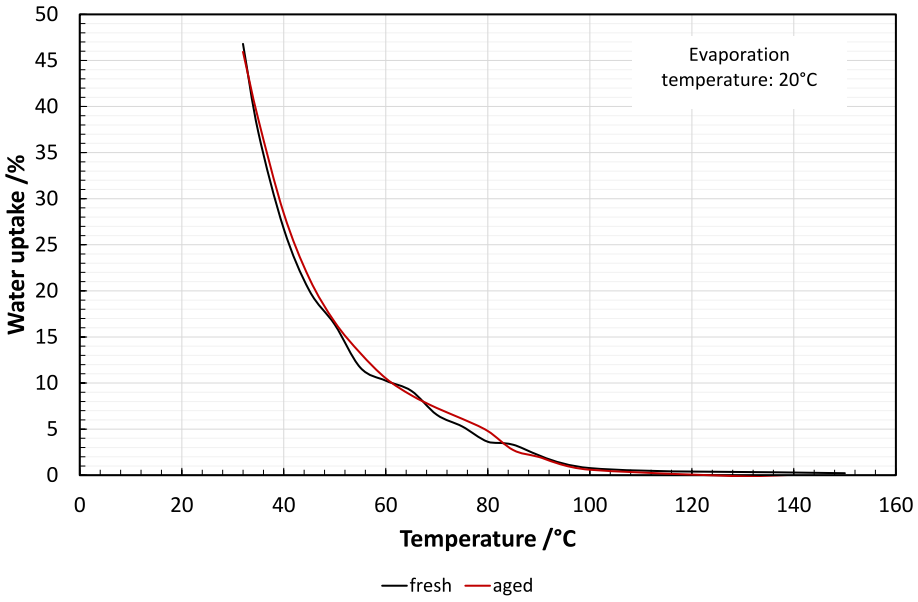

Fig. 2. Comparison of fresh and aged material.

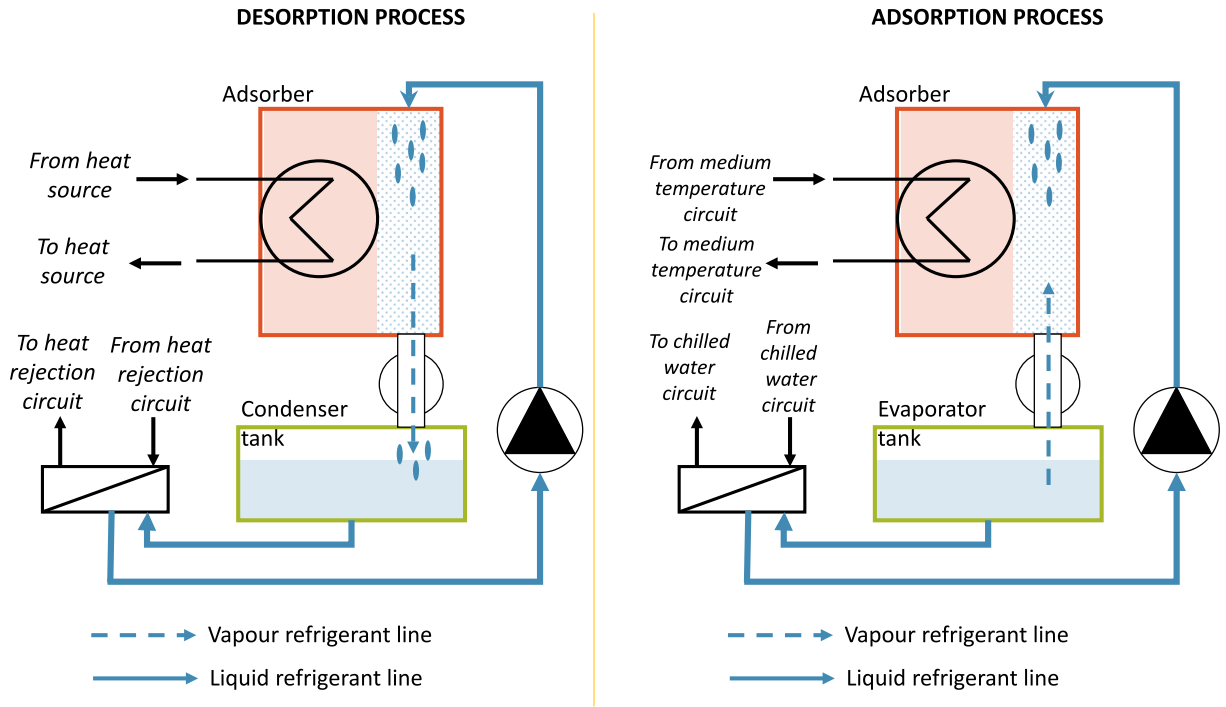

Fig. 3. Operating principle of the sorption device tested.

3.2. *Prototype development and manufacturing*

The prototype was realized according to the operating principle presented in the previous section. The detailed layout of the prototype is shown in Fig. 4. It consists of two adsorber modules, adsorber module 1 (M1) and adsorber module 2 (M2), which are operated in counterphase, i.e. while one is in the desorption/condensation phase, the other is in the adsorption/evaporation phase, to guarantee a quasi-continuous heating/cooling provision. The modules are connected to the condenser tank and evaporator tank by means of pneumatically actuated valves. The refrigerant pumps (condenser pump and evaporator pump) are side channel pumps. The two HEXs connected to the condenser and evaporator circuits are both plate HEXs. The adsorber modules are fin and tube HEXs containing the composite material inside, which is kept in place by using a metallic mesh. Moreover, in each adsorber vessel, there are two sections with a porous structure or PC onto which the refrigerant is dropped; one section is connected to the condenser tank (orange circuit) and the other to the evaporator tank (purple circuit). The hydraulic circuit of the fin and tube HEX is connected to three-way valves, that allow the connection to the High Temperature (HT) circuit during desorption phase and to the Medium Temperature (MT) circuit during adsorption phase. The condenser HEX is connected to the MT circuit as well, in parallel with the adsorber modules, whereas the evaporator HEX is connected to the Low Temperature (LT) HTF-circuit. The prototype is equipped with all the necessary sensors for the evaluation of its performance, namely pressure sensors on both adsorber modules,

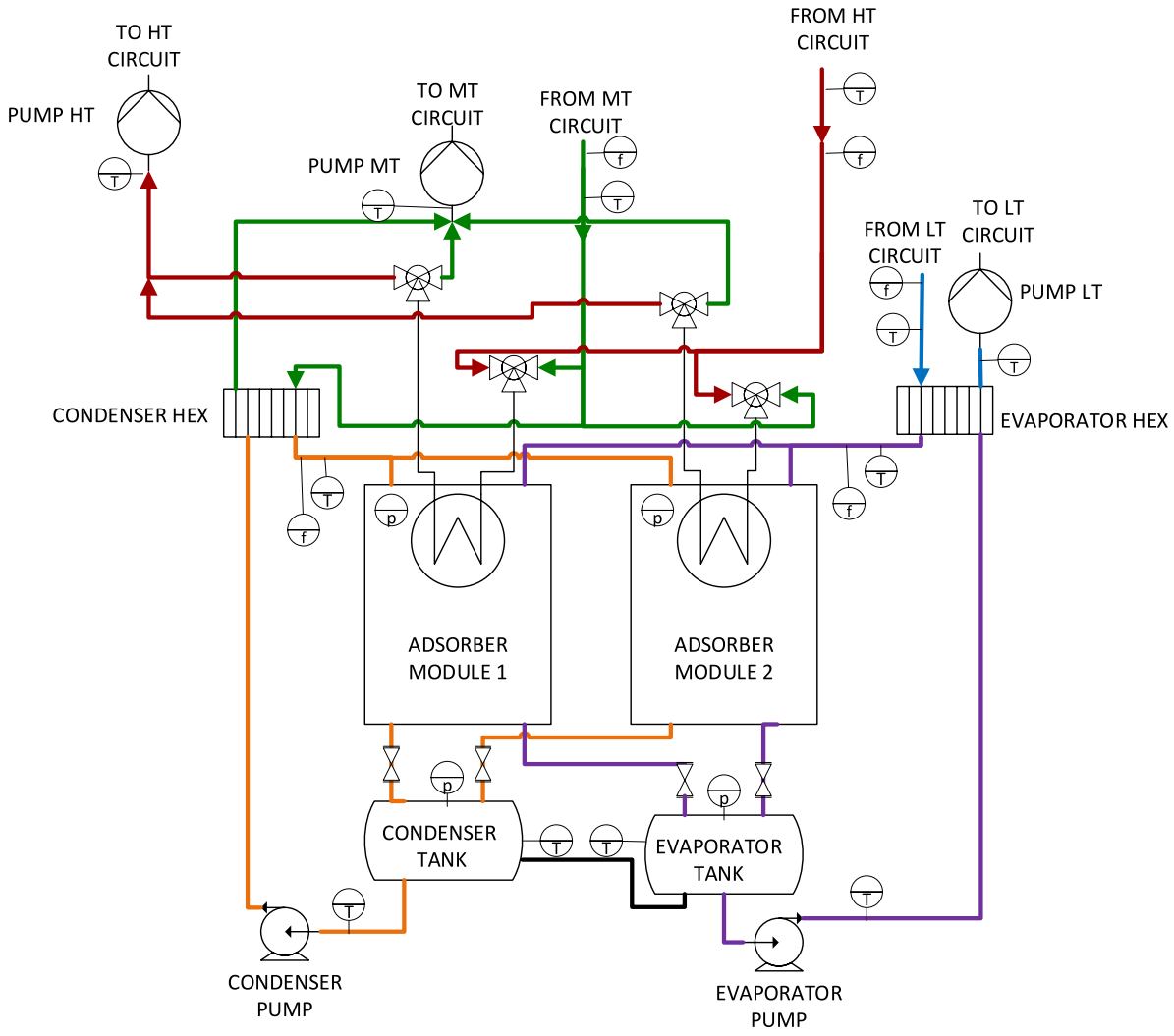

Fig. 4. Detailed layout of the prototype tested, including the main components and sensors. the different colours indicate the different circuits.

temperature sensors installed in the three circuits of the HTF (HT, MT, LT), as well as in the condenser and refrigerant circuits within the machine. The flow rate is measured for the three circuits of the HTF (HT, MT, LT) as well as on the condenser and evaporator circuits. By installing the temperature sensors and flow rate sensor also in the refrigerant circuits (condenser and evaporator), a direct measure of the thermal power supplied/released to/from of the material is possible, neglecting the efficiency of the external HEXs, for an evaluation of the actual potential of investigated sorbent material and the configuration with direct evaporation/condensation.

The list of installed sensors, type and accuracy is given in Table 4.

The manufactured prototype is shown in Fig. 5, whereas Fig. 6 shows a detail of the adsorber HEX with the composite material. The prototype is realized by placing the two modules on top of the condenser and evaporator tank, slightly tilted with respect to the floor. This choice was made to improve the efficiency of the condensation/evaporation inside the modules, by guaranteeing the proper flow of refrigerant. All the components are insulated by means of polyurethane foam with 10 mm thickness. The three-phase pumps used are controlled in speed by adjusting the power frequency, both in the HTF circuits and in the refrigerant circuits.

The main specifications of the prototype are listed in Table 5.

Table 4
List of sensors in the prototype and their accuracy.

Sensor	Measured value	Accuracy
Capacitive ceramic pressure sensor VCC200MA4	Pressure inside adsorber modules 1 and 2	±0.25 %
Magnetic-inductive flow meter MVM-250-PA	Water flow rate in HTF circuits	±1.5 %
Vortex flow meter G1M-AS009	Water flow rate in condenser and evaporator circuits	±1 %
PT1000 temperature sensors	Temperatures at inlet/outlet of the machine on the high-pressure side (HTF circuits), temperatures at inlet/outlet of the machine on the vacuum side (condenser and evaporator circuits), temperatures in the condenser and evaporator tanks.	±0.5 °C

4. Experimental

4.1. Testing facilities

The prototype was tested using a dedicated testing rig provided by Sorption Technologies GmbH in Germany. It allows to supply the prototype with the necessary HTF-circuit, namely HT, MT and LT streams. The heat source (HT circuit) is supplied by a 0.6 m^3 water tank,

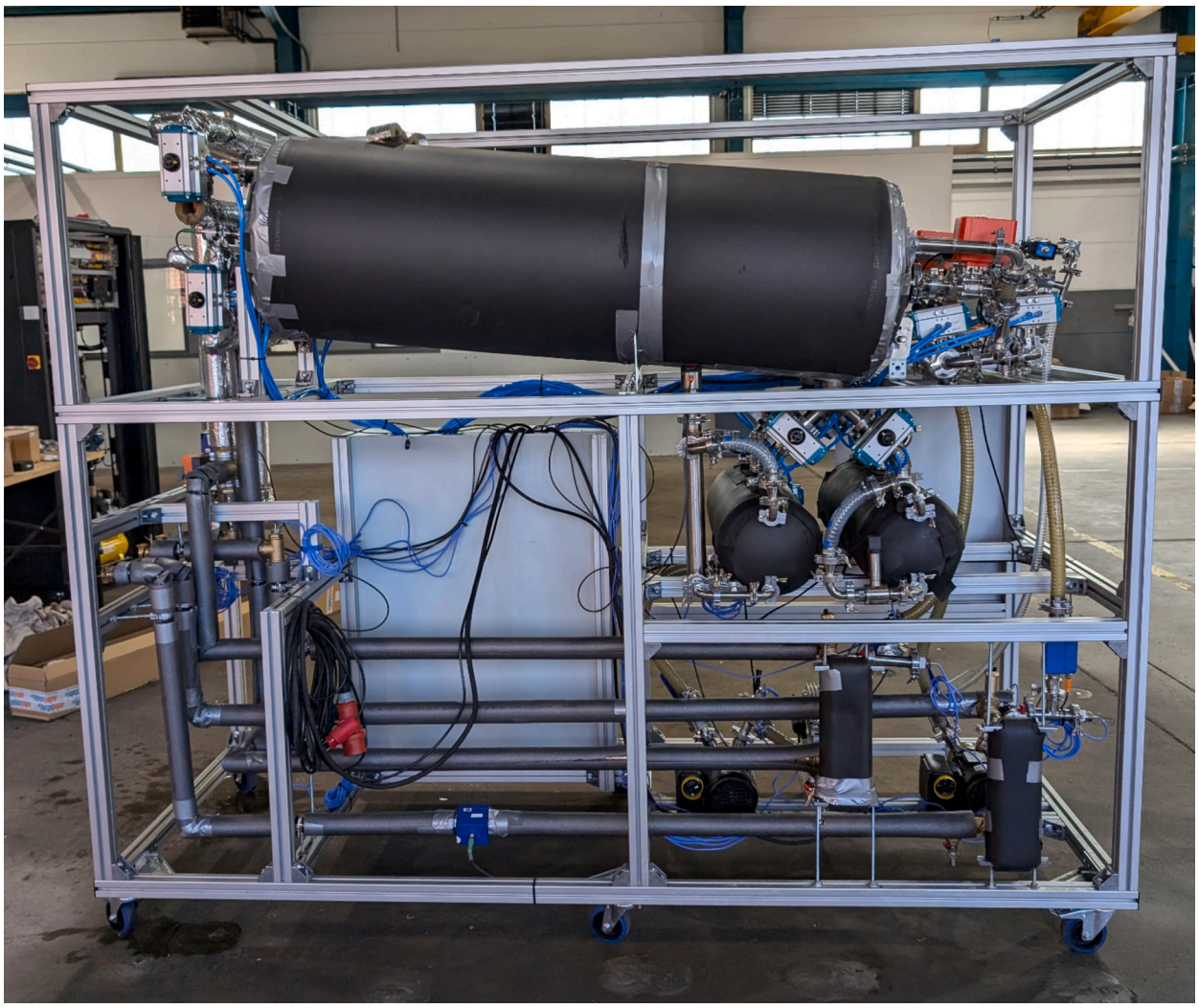

Fig. 5. Manufactured prototype (side-view). The tilted cylinder on top is one of the two adsorbers modules; on the left the hydraulic connections with the customer; on the right the vacuum circuit.

Fig. 6. Detail of the adsorber, including the heat exchanger, 38 kg of sorbent and a surrounding structure able to keep the material inside.

Table 5
Main specifications of the prototype.

Parameter	unit	value
Overall dimensions	m × m × m	2.1 × 0.99 × 2.46
Adsorber modules overall volume	m^3	0.23 (each)
Condenser/Evaporator tank volume	m^3	0.025 (each)
Condenser/Evaporator HEX heat transfer area	m^2	0.48 (each)
Overall amount of sorbent	kg	75 kg
Overall amount of refrigerant	kg	40
Adsorber HEX, fin pitch	mm	3.5
Adsorber HEX, fin height	mm	330

connected to an electric heater with overall power of 62 kW. The MT circuit of the prototype is connected to a 1 m^3 water storage, whereas the LT circuit is connected to a 0.6 m^3 water storage. Both the MT and the LT tanks are connected to a dry cooler with a maximum capacity of 93 kW. The temperature of LT-tank is maintained constant by mixing the right amount of water from the MT-tank using an electrically controlled valve (DV1) and Pump P6 in order to warm it up, while the MT-tank is cooled using the dry cooler. The dry cooler runs on a separated water loop, which only exchange heat with the MT circuit by means of a plate HEX. All the circuits are equipped with variable speed pumps and, on each circuit, there is a dedicated expansion vessel. Air vents and temperature sensors are installed in all the circuits. The P&ID of the testing rig is shown in Fig. 7.

4.2. Testing procedure

The testing procedure consists of the following steps:

1. Starting the electric heater and the pumps on the control side of the testing rig.
2. Starting the dry cooler.
3. Setting the temperatures in the tanks according to experimental design, the LT condition is reached by letting the machine run with the valve DV1 closed and pump P6 off.
4. Once the desired temperature on HTF-circuit is reached, the pumps connecting the testing rig to the prototype are started i.e. pumps P1, P2 and P3 for corresponding HT, MT and LT streams.
5. The prototype is run for at least three (3) cycles with long desorption times (1200 s), or the cycles needed for the LT-tank to reach desired temperature.
6. If needed, evacuation is carried out.
7. Starting of the test. Each test is recorded for at least three (3) full cycles after having steady-state conditions.

4.3. Testing conditions and data analysis

As mentioned in sections 1 and 2, the composite material selected SG-25 %$CaCl_2$ for the prototype is usually analyzed in the literature for thermochemical storage applications. However, materials belonging to the same class of "salt in porous matrix" were also considered for air humidification/dehumidification and in thermal desalination systems. In the current study, the majority of tests were dedicated to the verification of operation under chiller conditions. However, this paper covers dedicated tests in "storage mode". All the results will be discussed and compared to other systems in the literature in the next sections.

The operating conditions tested as a chiller machine are summarized in Table 6.

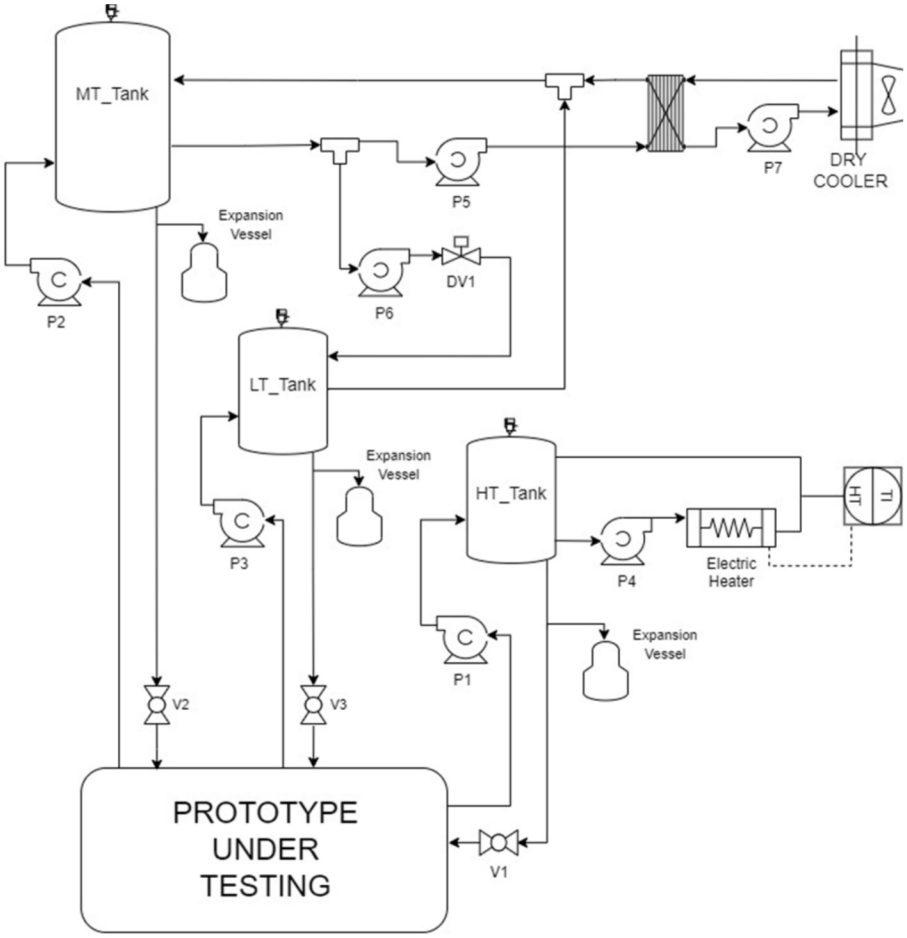

Fig. 7. P&ID of the testing rig for the prototype.

Table 6
List of testing conditions.

HT [°C]	MT [°C]	LT [°C]	cycle time	flow rates (HT – MT – LT) [kg/s]
85 °C	28, 30, 35	12, 16, 20	800, 1200	0.90 – 0.60 – 0.35

The HT inlet was selected as the most suitable temperature for the proper regeneration of the material according to the equilibrium curves reported in Fig. 1. The MT temperatures selected are representative of different operating conditions when connecting the chiller to an external rejection circuit in a warm climate, whereas LT temperatures were selected as the typical operating points in high-temperature cooling distribution systems, which represent the best operating scenarios for thermal chillers [19].

Starting from the measured data, the thermal power in the various hydraulic circuits (HTF and refrigerant) was calculated as:

$$\dot{Q} = \dot{m}\, c_p (T_{in} - T_{out}) \tag{1}$$

where $\dot{Q}$ [kW] is the thermal power, $\dot{m}$ [kg/s] is the mass flow rate, c_p [kJ/(kg K)] is the specific heat of water, T [°C] is the temperature and "in" and "out" stands for inlet and outlet of each circuit.

The energy for each circuit was calculated as the integral of the power:

$$Q = \int_0^{t_{fin}} \dot{Q} dt \tag{2}$$

where Q [kJ] is the energy and t_{fin} [s] indicates the final time of each test.

The thermal COP for chiller mode was calculated as the ratio between the energy withdrawn from the LT circuit and the energy supplied in the HT circuit:

$$COP = \frac{Q_{LT}}{Q_{HT}} \tag{3}$$

In addition, for the tests in chiller mode, the EER was calculated as the ratio between the cooling energy and the energy due to the consumption of electric devices, i.e. the refrigerant pumps and the PLC.

$$EER = \frac{Q_{LT}}{E_{auxiliaries}} \tag{4}$$

5. Results

5.1. Typical trends during operation

Fig. 8 shows the temporal evolutions of the temperatures in the HTF circuit. HT_in (black line), MT_in (green line) and LT_in (blue line) are the inlet temperatures from the testing rig, which remain stable at 85 °C, 30 °C and 16 °C respectively. The outlet temperatures of the three circuits follow the typical trends of an adsorption chiller: HT_out increases rapidly at the beginning of the phase (when the heat contribution is mostly used for heating up of the material) and subsequently increases more slowly when desorption starts. When changing the steps of the cycle, the temperature drops due to the switching of the valves from the HT to the MT circuit. The same comments can be made for the MT_out, that has a spike at the beginning of each cycle step and then drops when condensation is almost completed. Regarding LT_out, it reflects the low-temperature side cooling effect, decreasing rapidly at the beginning of the adsorption and then remaining relatively stable during the entire phase, thus supplying a continuous cooling effect.

It is worth noticing that there is an apparent asymmetry in the operation of the two modules: as it can be seen in Fig. 8, when the module 1 ends desorption and the subsequent operation starts, then the HT_out temperature is approximately 55 °C, whereas at the end of the desorption of module 2 it approximately 45 °C. Moreover, LT_out temperature also exhibits a slightly different behavior (with two distinct peaks in one case). This is due to the organization of the cycle for the specific prototype: beside the two phases (1 and 3), where adsorption in one module and concurrent desorption in the other module, there are the two isosteric heating/cooling phases (phase 2 and phase 4) and an extra phase, called phase 5. This is peculiar for the specific architecture of this prototype and it is a short phase during which the two tanks for the refrigerant are connected to equalize their levels and allow for safe operation.

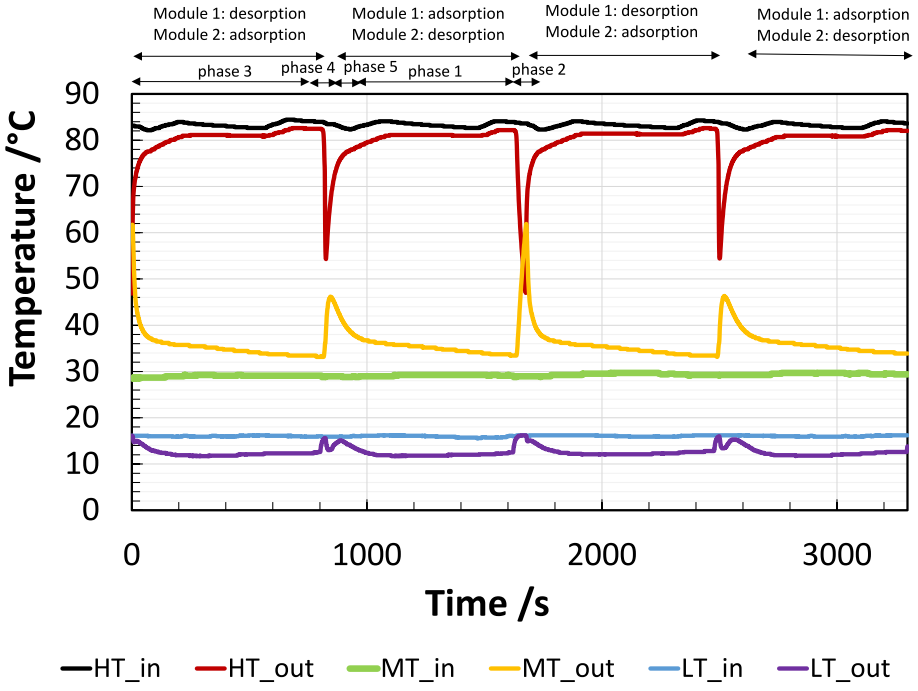

Fig. 8. Typical temporal evolutions of the circuits for the HTF during a test.

Fig. 9 illustrates the temperature trends in the low-temperature side (Evaporation loop) for the same test, with a focus on both the external cooling circuit and the internal working refrigerant (water). The temperatures measured are associated with the operation of the adsorption/evaporation; both the external load (LT_in and LT_out values) and the working fluid (Refrigerant or "RefEV") data is reported. LT_out represents the temperature of the heat transfer fluid exiting the system, which is basically constant at 12 °C with the exception of the transition steps. The peaks in the temperatures, which are better highlighted in Fig. 9 than in Fig. 8, represent the isosteric heating/cooling phases of the cycle. The evaporator tank temperature (EV_tank, grey), is measured in the lower part of the tank, follows closely the outlet temperature of the refrigerant, which is measured right after the suction line of the refrigerant pump. In Fig. 9, it was highlighted that the actual temperature difference in the refrigerant circuit is 6 K, whereas the temperature difference between the outlet temperature of the refrigerant and the outlet temperature of the heat transfer fluid is approx. 3.5 K, which indicates an efficient operation of the plate EV_HEX.

Fig. 10 shows the temporal evolutions of temperatures on the medium temperature side of the chiller. It is worth remembering that the MT circuit of the HTF is connected both to the condenser and to the module that is undergoing adsorption, as illustrated in the P&ID of the prototype in Fig. 4. This explains the high peaks with large temperature variations in the MT_out line, which are due to the switching of the valves between the two circuits. As for the circuit of the refrigerant on the evaporator side, also in this case, the temperature of the condenser tank (measured at the bottom of the tank), is almost identical to the temperature of the refrigerant outlet. The actual temperature difference on the refrigerant circuit is 7 K, therefore similar to the one on the evaporator side.

Fig. 11 shows the temperature evolutions in the two adsorption modules (solid lines), compared with the pressure for water at liquid/vapour equilibrium (dashed lines), which were calculated from the temperatures inside the condenser and evaporator tanks using the equations already implemented in CoolProp [20]. It is possible to notice that, for basically the entire cycle duration, the pressure measured in the modules correspond to the pressures at equilibrium. This behaviour indicates that the desorption/condensation and adsorption/evaporation process occur correctly and in an efficient way. On the contrary, an increased pressure, especially during condensation, can indicate an undersized component. At the beginning of desorption/condensation there is indeed a temporal shift between the peak in the pressure measured in the module and the one in the tank, which is due to the time needed for the condensed vapour to reach the condenser and determine the increase in pressure.

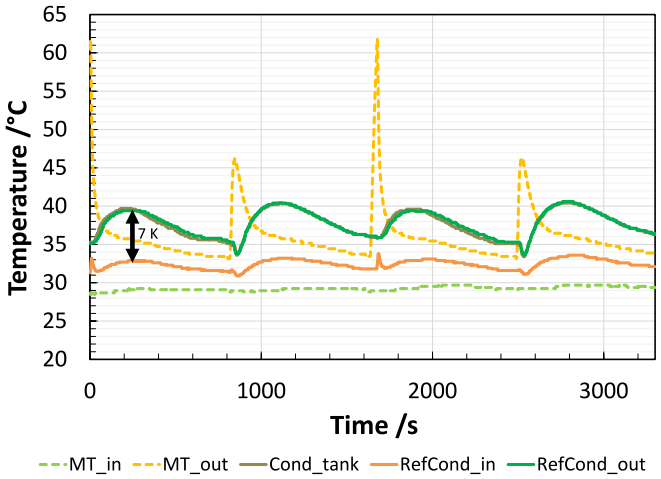

Fig. 10. Typical temporal evolutions of the temperatures in the circuits in the condenser and MT side during a test.

Finally, Fig. 12 shows the thermal powers measured in all circuits. The HT power and MT power have very high peaks at the beginning of each step of the cycle, due to the switch between the two hydraulic circuits exhibiting a large temperature differences. The green line (Q_CD) and purple line (Q_EV) refer to the powers measured in the refrigerant circuit. The power measured in the condenser circuit cannot be directly compared to the power measured on the HTF side of the plate HEX because the MTin and MTout sensors are installed after the junction between the two MT streams, the one going out the condenser plate HEX and the other exiting the adsorption module. Instead, a comparison can be made on the LT/EV side: the two powers are very similar, with a calculated efficiency of the plate HEX of 90 %.

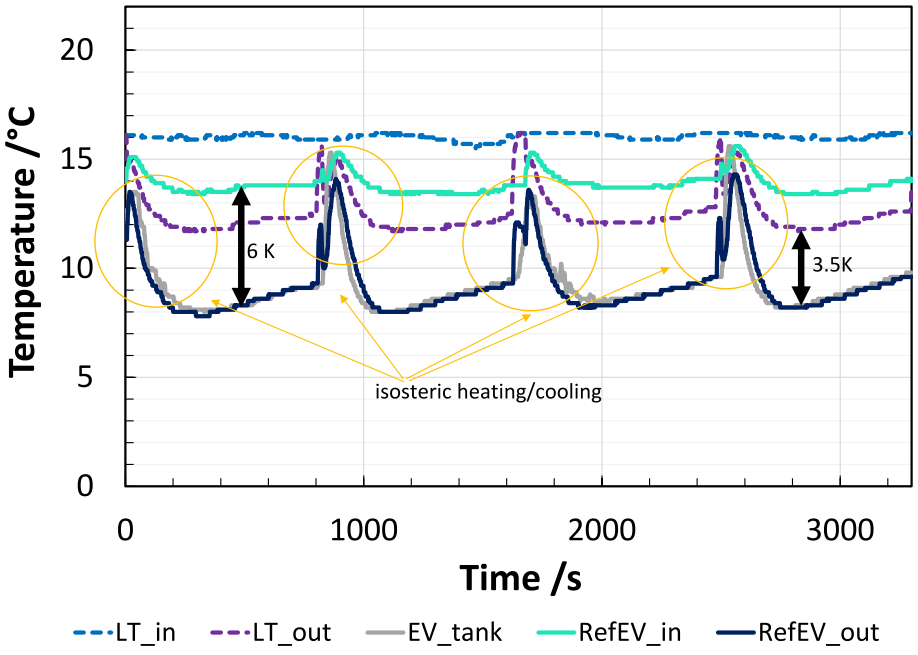

Fig. 9. Typical temporal evolutions of the circuits in the evaporator and LT side during a test.

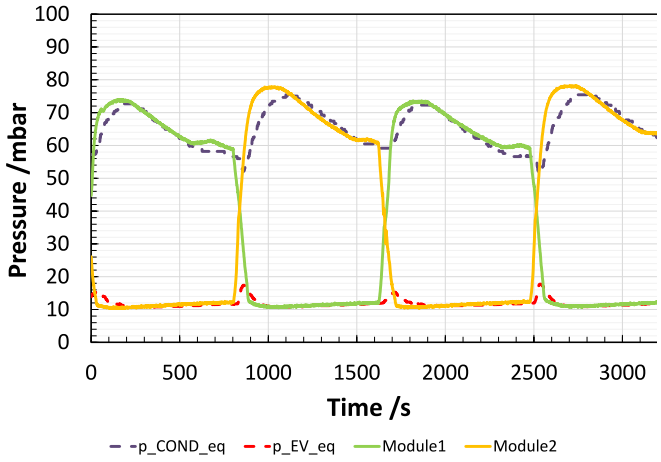

Fig. 11. Typical temporal evolutions of the pressures.

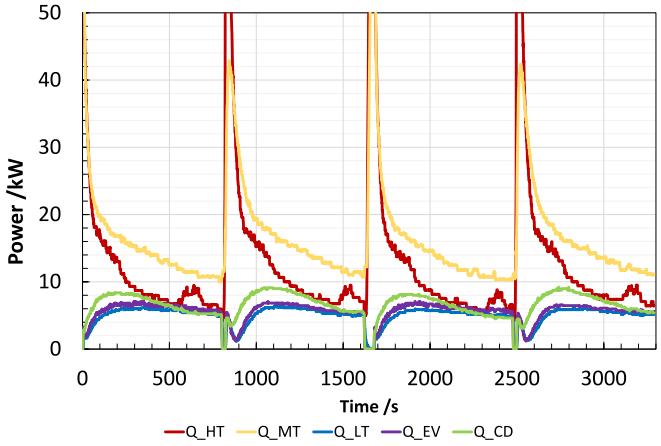

Fig. 12. Typical temporal evolutions of the thermal powers in all circuits.

5.2. Results for chiller mode

The data from the tests carried out was analyzed by evaluating the thermal coefficient of performance (COP) and cooling power as a function of the temperature lift, which was calculated as:

$$T_{lift} = Refr, cond_{out} - Refr, ev_{out} \quad (5)$$

Indeed, as widely reported in the literature [19], the temperature lift between the working fluid at the evaporator and at the condenser can be assumed as the lift between the hot and cold source temperatures for a heat pump and therefore a measure of the driving force for the process. Fig. 13 shows the cooling power and thermal COP as a function of the temperature lift. Fig. 13a illustrates the relationship between cooling power and temperature lift. The experimental data points indicate a clear inverse relationship between the cooling power and the temperature lift. As the temperature lift increases from approximately 27 K to 32 K, the cooling power decreases from values approaching 8 kW to nearly 2 kW. This trend is captured by a linear regression with an R2 value of 0.9227, indicating a strong correlation and providing confidence in the reproducibility of the experimental data. The declining trend is typically observed in this kind of systems and aligns with experimental findings from the literature: the higher temperature lift results in a lower amount of refrigerant exchanged during the cycle and therefore in a reduced system's cooling capacity.

Fig. 13b shows the trend for the thermal (COP) of the tested adsorption chiller as a function of the temperature lift. The plot shows a clear inverse relationship between thermal COP and temperature lift, similarly to the trend from Fig. 13a. At lower temperature lifts, around 25 K–26 K, the COP reaches values close to 60 %. As the temperature lift increases to about 30 K, whthe COP drops to approximately 35 %. This decline is consistent with the thermodynamic behavior of adsorption chillers, where higher temperature lifts require more energy input to maintain the same cooling output, thereby reducing the system's overall efficiency. Furthermore, the figure's linear regression suggests that while the system operates efficiently at low temperature lifts, COP degradation becomes more pronounced as the temperature lift increases.

Fig. 14a shows more in detail the effect of MT inlet and LT inlet on the cooling capacity delivered by the prototype. It is possible to notice that, while for LT_{inlet} of 16 °C and 20 °C, passing from 25 °C to 35 °C of MT_{inlet} only corresponds to a decrease in cooling power of approx. 20 %, for LT_{inlet} of 12 °C, the reduction is of 50 %. The system performs best when the LT inlet temperature is the highest (20 °C) and the MT inlet temperature is low (around 26 °C), yielding the highest cooling power. Conversely, when both the LT and MT inlet temperatures are high, the system exhibits lower cooling power, as seen in the case of LT_in = 12 °C, where cooling power falls to nearly 2 kW at 34 °C.

Fig. 14b shows the COP and EER for the same set of tests. The EER

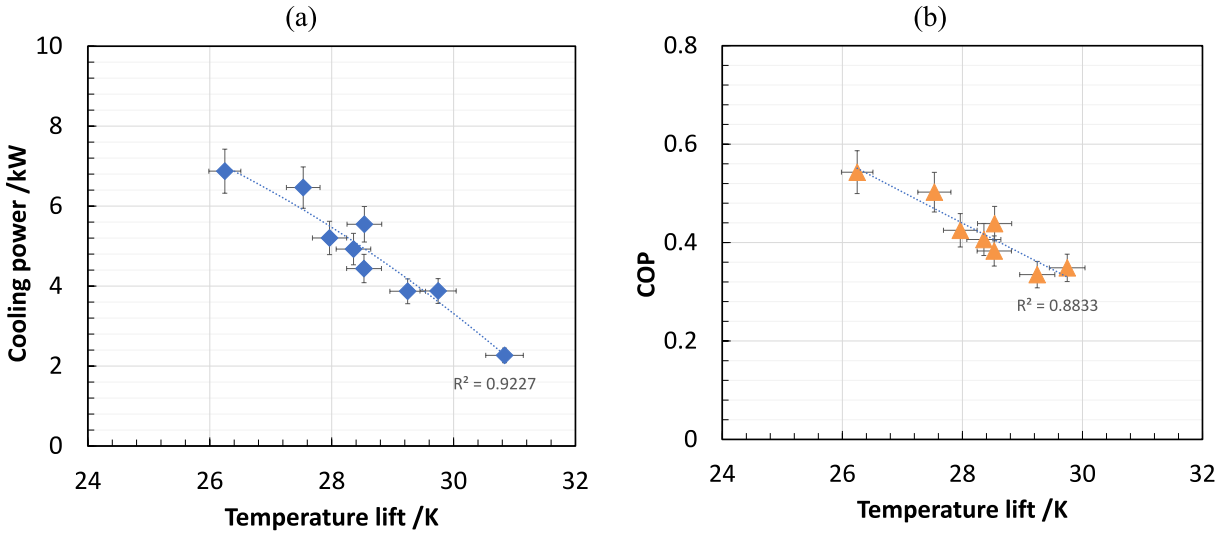

Fig. 13. Cooling power (a) and cop (b) for the tested prototype as a function of the temperature lift.

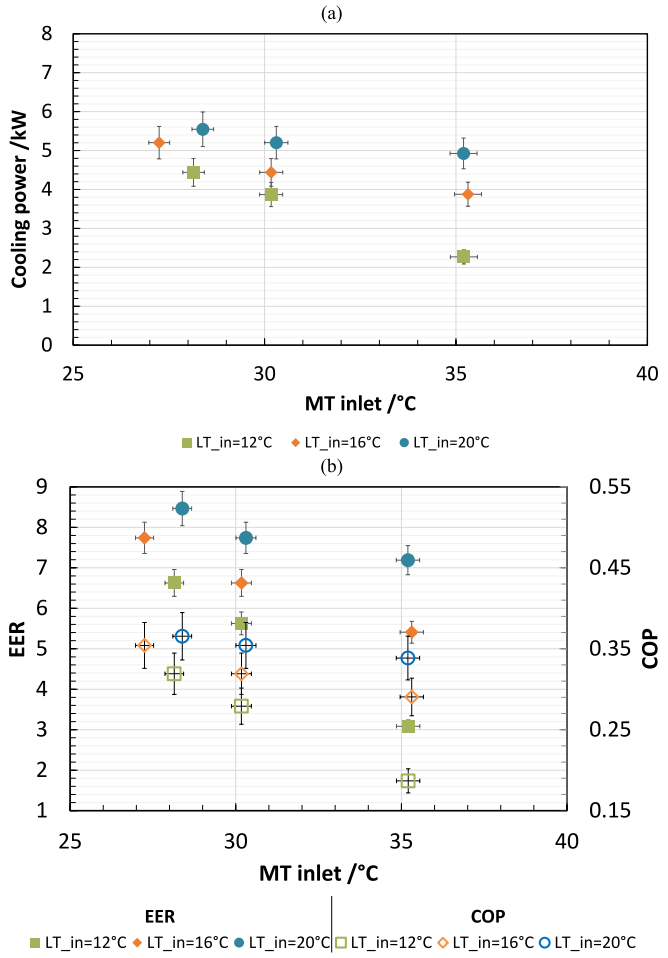

Fig. 14. Effect of HTF circuit temperatures on cooling power (a) and COP and EER (b)r.

(filled symbols, left axis in the figure) ranges between 8.6 and 5.5, with the only exception of the test with inlet temperature to the evaporator circuit of 12 °C and 37 °C inlet temperature to MT circuit. The COP (blank symbols, right axis) is in the range 0.17–0.37. It is worth noticing that, despite theoretical COP for such systems are usually in the range of 0.40 to 0.60, there are not many experimental proofs of large-scale systems that can reach such values. This is mostly due to the large thermal masses of the heat exchangers. On the contrary EER values are quite high, which is due to the presence of only two pumps for the refrigerant, which are also operated at low rotations.

5.3. Results for storage mode

As previously discussed, the main aim of the experimental campaign was to verify the system's performance in chiller mode, but, considering the wide use of the employed sorbent as a thermochemical energy storage material, some tests were dedicated to the verification of the potential as a storage. To this aim a possible application was identified, which corresponds to charging with a high temperature heat pump, e.g. for sector coupling applications. It was considered to have condensation and adsorption in the range 30–35 °C, which corresponds to the typical temperature lift for a low-temperature residential heating system. At the same time, 12–7 °C (inlet–outlet) were considered on the low temperature side, thus allowing also to verify the possible use as a cold storage coupled to a typical cooling distribution system.

The temperatures of the HTF circuits during the adsorption/evaporation process for one of the modules are reported in Fig. 15. The test was carried out until the temperature difference between the inlet and outlet of each HTF circuit was lower than 1 K, which resulted in an overall time for adsorption of 3800 s.

The results of tests in storage mode are synthetically shown in Table 7, where the average values for the two modules are reported. It is worth noticing that the overall storage capacity is the sum of the two modules so approx. 30 MJ, corresponding to 8.3 kWh, in cold storage operation, and 39 MJ, corresponding to 10.8 kWh as heat storage.

All the results obtained in this section will be critically discussed in the next section, comparing them to the results of other state-of-art prototypes in the literature to define whether the system is effectively performing.

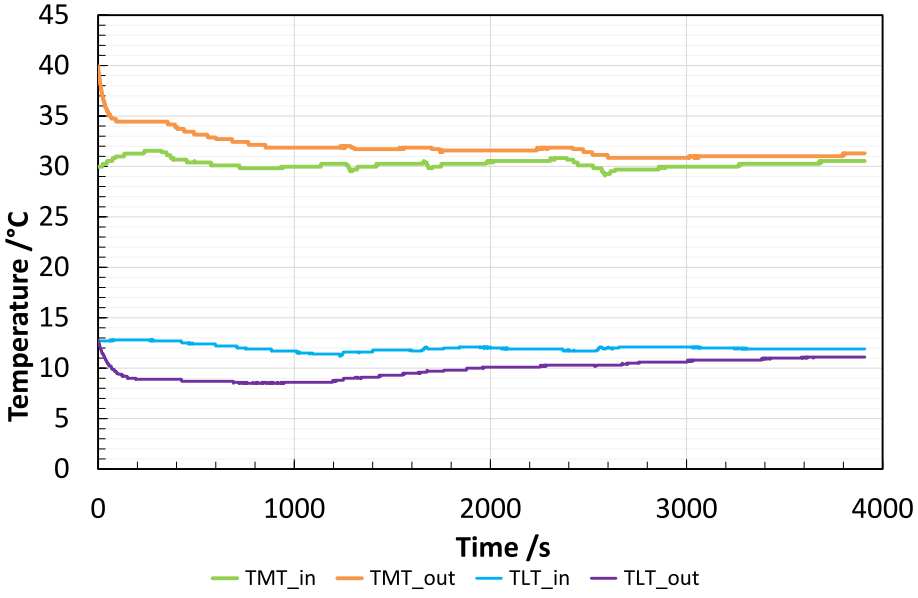

Fig. 15. Temperatures during adsorption of module 2 for storage mode.

Table 7
Results of tests in storage mode.

Test	Q_MT	Q_LT	Energy_charged	Energy_discharged_MT	Energy_discharged_LT
	kW	**kW**	**MJ**	**MJ**	**MJ**
M1_charge	3.7	–	22.5	–	0.0
M1_discharge	3.7	2.7	0.5	19.2	14.5
M2_charge	4.5	–	22.6	–	0.0
M2_discharge	4.3	3.1	0	19.6	14.9

6. Discussion

6.1. Heat transfer evaluation

The first analysis carried out was on the heat transfer coefficient for the condensation and evaporation processes. As mentioned in section 3.1, one of the innovative features of this prototype is the use of a different approach for the evaporation/condensation processes, which occur inside the adsorber module by letting the fluid refrigerant flowing through a porous structure.

In order to assess this choice, the overall heat transfer conductance was calculated as:

$$UA_{cond(evap)} = \frac{\dot{Q}_{cond(evap)}}{LMTD} \tag{6}$$

where UA [W/K] is the overall heat transfer conductance, $\dot{Q}_{cond(evap)}$ [W] is the thermal power during the condensation or evaporation process measured in the refrigerant circuit, LMTD [K] is the logarithmic mean temperature difference, which was calculated as:

$$LMTD = \frac{T_{ref_{in}} - T_{ref_{out}}}{ln\left(\frac{T_{ref_{in}} - T_{sat}}{T_{ref_{out}} - T_{sat}}\right)} \tag{7}$$

where $T_{ref_{in}}$, $T_{ref_{out}}$ are the temperatures of the liquid refrigerant and T_{sat} is the saturation temperature calculated from the pressure inside the modules, which is an indication of the temperature of the vapour evaporating/condensing. The calculation was carried out using the equations implemented in CoolProp.

It is worth mentioning that it is not possible to know which is the active area involved in the condensation/evaporation over the porous structure and therefore it is not possible to separate the terms U (overall heat transfer coefficient) and A (overall heat transfer area). Moreover, the value UA is not constant for the entire duration of each step of the cycle, but for comparison's sake, the average value over each test was considered. The results are reported in Fig. 16a for the condensation process and in Fig. 16b for the evaporation process. In order to simplify the comparison with previous results related to the cooling power, the results are organized considering the different external operating boundaries (MT_{in} and LT_{in}). The results show that the effect of inlet chilled water temperature (and, consequently, refrigerant temperature at the evaporator) are influencing the results significantly. This can be explained by the low pressure level at which the evaporation process occurs, that changes only slightly among the different tests. Instead, the increasing cooling water temperature leads to a reduction in the heat transfer coefficient. In this case, the dominating effect is the reduced amount of refrigerant adsorbed/released at the higher adsorption temperatures, rather than the condensation/evaporation technology. The UA for the adsorption/evaporation process is slightly lower than the one measured during condensation (approx. 20 % lower). This effect has been widely discussed in the literature [21,22] and it is due to the sub-atmospheric pressure conditions in which the process occurs, that are penalizing heat transfer: since evaporation occurs at lower pressures than condensation, the resulting heat transfer coefficient is lower.

It is also interesting to compare the results obtained with similar studies in the literature regarding evaporators for sorption chillers. Configuration studied in the literature, and compared to the current system, include fin and tube heat exchangers in pool boiling configuration, capillary-assisted evaporators, plate heat exchangers and falling film evaporators. The comparison is reported in Table 8, where only the conditions comparable with the current study are considered for a reasonable evaluation. When multiple configurations and operating

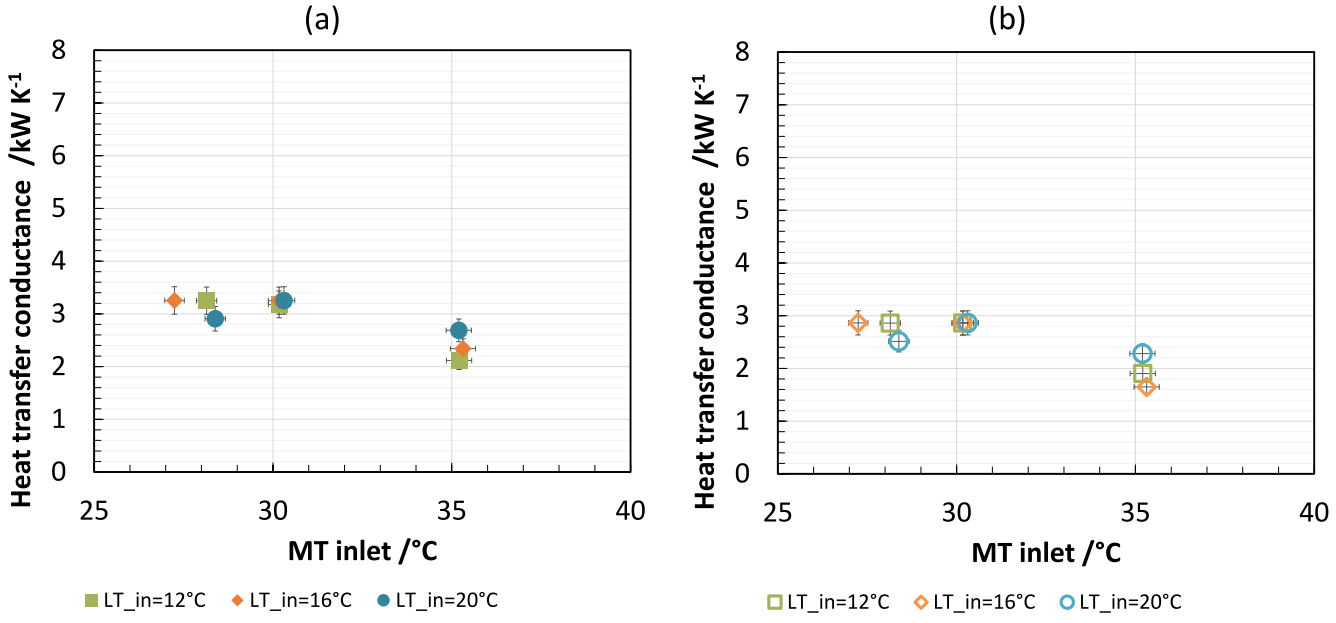

Fig. 16. Heat transfer conductance for adsorption and desorption tests in chiller mode; (a) during condensation, (b) during evaporation.

Table 8
Comparison of heat transfer conductance with other literature studies.

Type of evaporator	Reference	Operating conditions	UA
Falling film system inside adsorption chamber	**This work**	**MT_in 30 °C, LT_in16°C**	**3 kW/K**
Fin-and-tube HEX – pool boiling	[23]	LT_in 25 °C, 90° inclination, 20 kg/min	1 kW/K
Fin-and-tube HEX with copper coating and Z-type turbulator– pool boiling	[24]	LT_in 15 °C, 2.5 kg/min	0.2 kW/K
Fin-and-tube HEX with fin spacing of 1.6 mm– capillary-assisted evaporation	[25]	LT_in = 23 °C, LT_out = 19 °C	0.6 kW/K
Finned pipes – capillary assisted evaporation	[21,22]	LT_in 15 °C	0.6 kW/K
Asymmetric plate HEX	[26]	LT_in 15 °C, MT_in 30 °C	1.4 kW/K
Falling film evaporator	[27]	LT_in = 15 °C	0.6 kW/K

conditions were reported in the references, only the best case was considered for evaluation. It is possible to notice that the values reported in this study are much higher than the other studies in the literature, up to 2 times higher than the best values measured in similar conditions so far, which correspond to the use of asymmetric plate HEXs. As mentioned previously, this is mainly due to the direct evaporation/condensation and by the continuous dropping of liquid refrigerant over a continuous porous structure. Moreover, since the evaporation and the condensation occur all along the adsorber length, the actual active area for the process is larger than when they occur in a separate chamber.

6.2. Comparison with other chillers in the literature

The results obtained in the present study were also compared to the results from other prototypes of adsorption chillers in the literature. There is an extensive amount of adsorption chillers developed over time, but it was decided to consider the systems that were compliant with the following criteria: (a) the reported performance is experimentally measured, numerical studies were not taken into account; (b) the results were published in the last 10 years; (c) the chiller should be developed exclusively for cooling applications, i.e. systems devoted to desalination + cooling were not considered in the comparison.

The studied reported in the literature are reported in Table 9. It is possible to notice that the vast majority of studies, even in recent years, are focusing on silica gel-water systems, whereas there is only one experimental proof of a chiller that is employing an adsorbent of the same type of the one used in the present study. The achieved COP is higher than experimental COP achieved by the other prototypes in the literature in similar operating conditions. This indicates that the selected layout allows an efficient exploitation of heat. It is also worth noticing that some of the other chillers used for comparison are exploiting optimization strategies such as heat and mass recovery [28] and continuously variable cycle times and flow rates [29], still reaching a COP approx. 20 % to 50 % lower than the one measured in the current study.

One of the main critics linked to the use of salt hydrates in large-scale systems is their slow dynamics and consequent reduction of average cooling or heating output achievable [30]. However, the results achieved in the current system demonstrate that the SCP is in line with the values achieved by standard refrigerants, such as silica gel. Indeed, the values reported in the current paper is slightly higher than those of silica gels from references [31] and [29], but the values from the silica gel prototypes refer to lower HTin.

6.3. Comparison with other thermal storages in the literature

The data for the tests of the prototype under heat storage mode were also compared to the ones reported in the literature. For the comparison, the same approach as for the case of chiller mode was used: (a) only experimental studies are considered, numerical studies only are discarded from the analysis; (b) studies published in the last 10 years only are considered; (c) the temperature levels should be comparable with those reported in the current studies; (d) only closed-cycle systems are considered for an assessment based on fair basis. It is important to remark that there is only a very limited amount of studies that analyse the storage performance in lab-scale, the vast majority of studies concerning thermochemical heat storage are dealing with material preparation and characterization or simulation of reactors. The thermochemical storage system comparison is presented in Table 10. It is possible to notice that the energy storage density achieved is one order of magnitude higher than that of FAM Z02 and of the other prototype reported in the literature that is using the pure salt hydrate ($SrBr_2$), whereas it is comparable with the energy storage density of the prototype using $MnCl_2$-NH_3 working pair, which is however working at higher pressures than the one reported in this study.

Finally, it is worth discussing the possible cost of the current system. It is important to notice that, at the moment, there are no sorption storages on the market, thus making it complicated to evaluate the cost

Table 9
Comparison of results for chiller mode with recent prototypes in the literature.

Reference	Adsorbent	Application	System layout	COP	SCP [W/kg]
This work	**Mesoporous silica gel-25 % $CaCl_2$**	–	**Two beds with refrigerant tanks for condenser and evaporator and separate plate HEXs**	**0.51 @HT_in 85 °C, MT_in 30 °C, LT_in 16 °C**	**150 @HT_in 85 °C, MT_in 30 °C, LT_in 16°C**[b]
[31]	Silica gel	Ultra-low heat recovery for data center cooling	Two beds with a single evaporator and a single condenser	0.42 @HT_in 60 °C, MT_in 30 °C, LT_in 22 °C	108.4 @HT_in 60 °C, MT_in 30 °C, LT_in 22°
[29]	Silica gel	Non-linear control strategy in solar-based plants	Single bed with a single evaporator and a single condenser	0.25 @HT_in 70 °C, MT_in 30 °C, LT_in 10 °C	140 @HT_in 70 °C, MT_in 30 °C, LT_in 10 °C
[32]	Mesoporous silica gel-20 % LiCl	–	Two beds with a single evaporator and a single condenser	0.40 @HT_in 80 °C, MT_in 30 °C, LT_in 20 °C	41 @ HT_in 80 °C, MT_in 30 °C, LT_in 20 °C
[28]	Silica gel	Solar cooling	Two beds with a single evaporator and a single condenser, including components for heat and mass recovery	0.485 @HT_in 70 °C, MT_in 30 °C, LT_in 25 °C	140 @HT_in 70 °C, MT_in 30 °C, LT_in 25 °C
[33]	Zeolite 13X	Solar cooling	Two evacuated-tube based adsorbers with a single condenser and evaporator	0.46 – day/night operation	16.41 day/night operation
[34]	Du et al	Data center cooling	Two adsorbers with condenser in the same vacuum chamber and a single capillary-assisted evaporator	0.50 @HT_in 50 °C, MT_in 30 °C and LT_in 23 °C	NA – volumetric cooling power 2.5 kW/m^3

*NA: Not Available.

[2] The SCP is calculated on half of the overall adsorbent material, i.e. the one contained in each module, since the power is calculated as the average power on each module.

Table 10
Comparison of results for storage mode with recent prototypes in the literature.

Reference	Adsorbent	Application	System layout	Energy storage density	Charge/discharge power
This work	**Mesoporous silica gel-25 % $CaCl_2$**	–	**Two beds with refrigerant tanks for condenser and evaporator and separate plate HEXs**	**256 kWh/kg (heat storage), 193.33 (cold storage), 3.6 MJ/m^{3}reactor (heat storage), 2.4 MJ/m^{3}reactor**	**3.7 kW charge – approx. 3 kW discharge power**
[35]	Zeoilite 13X	Cold storage, open cycle	Single bed with a component working as condenser/ evaporator	NA	0.5 kW discharge power
[36]	Zeolite 13X	Heat storage for residential case, closed cycle	Single bed with a component working as condenser/ evaporator	20.4 kWh/m$^{3\ material}$ @150 °C/30 °C charging and 70 °C/40 °C discharging	NA
[37]	AQSOA FAM Z02	Thermochemical mobile storage for heating and cooling applications, closed cycle	Single bed with a component working as condenser/ evaporator	1.6 kWh/kg /short term heat storage), 2.8 kWh/kg (long-term heat storage), 0.8 kWh/kg (cold storage) @90/30 °C charge and 30/10 °C discharge. All density to be considered per kg of material	0.6 kW discharge power
[38]	Zeolite 13X	Solar-based seasonal storage for building applications, closed cycle	Two beds with a single condenser/evaporator and a refrigerant tank	178 kWh/m^{3}materil with 30 °C/20 °C discharge conditions	2 kW discharge power
[39]	$MnCl_2$-NH_3	Heat storage for building applications, closed cycle	Single bed with a component working as condenser/ evaporator	2.8 MJ/kg material with 174 °C/50 °C charge and 50 °C/20 °C discharge	NA
[40]	$SrBr_2{\cdot}6H_2O$	Heat storage for building applications, closed cycle	single bed with a component working as condenser/ evaporator	65 kWh/m^3 reactor with 100 °C desorption temperature and 15 °C adsorption temperature	0.62 kW discharge power

performance of the prototype. The cost of the material (considering only the raw components) is approximately 15 €/kg. According to the estimation from Sorption Technologies, assuming a scale up of the component to a 200 kWh storage, the estimated cost/kWh of the storage in serial production would be 1200 €/kWh. However, further replication studies would be needed to properly confirm such values.

7. Conclusions

The experimental investigation of the sorption system prototype presented in this study proved, in a realistic scale, the feasibility of the application of composites made with salt hydrates for large-scale sorption systems. The core of the study is the integration of a large amount (75 kg) of a composite material — specifically, silica gel impregnated with calcium chloride ($CaCl_2$)—in a prototype which employs a novel evaporation/condensation system, to prove the scalability of the concept.

The novel design of the adsorption reactor, featuring the flow of refrigerant in liquid form and the use of an external plate heat exchanger for evaporation and condensation, proved effective in optimizing heat and mass transfer. This design innovation addresses some of the critical challenges that have limited the scalability of previous sorption systems. By integrating a porous structure within the vacuum chamber, the system not only improved the compactness of the setup but also minimized thermal losses, further enhancing the system's overall performance. The heat transfer coefficient UA calculated in the conditions of this study is 3 kW/K, up to three times higher than the one of the best state-of-art evaporators/condensers developed in the literature for application in sorption systems.

The experimental results indicated that the system could deliver a notable cooling power, with an average output of up to 6 kW during chiller operation. This performance is competitive when compared to similar-scale systems documented in the literature, suggesting that the prototype is capable of providing effective cooling under typical operational conditions. Furthermore, the thermal energy storage capacity of the system was 14 MJ measured during cooling operations and 19 MJ during heat storage storage operation. These results confirm the capability of the composite material to achieve high energy density while maintaining operational flexibility, i.e. without substantial penalization due to the possible slow dynamics of the composite material.

It is then possible to conclude that the prototype's design and operational strategies provide a solid foundation for future development, with applications in real-world district heating and cooling (DHC) networks or building-scale thermal management systems. The findings of this study underscore the viability of composite materials and innovative reactor configurations in improving energy efficiency and flexibility in large-scale adsorption chillers. Such efforts are essential for enabling broader adoption of sorption systems in renewable energy grids and waste heat recovery applications.

CRediT authorship contribution statement

Valeria Palomba: Writing – original draft, Supervision, Software, Project administration, Methodology, Investigation, Funding acquisition, Data curation, Conceptualization. **Andrea Frazzica:** Writing – review & editing, Supervision, Methodology, Investigation, Conceptualization. **Vincenza Brancato:** Writing – review & editing, Validation, Investigation, Formal analysis. **Antonino Bonanno:** Investigation, Data curation. **Yannan Zhang:** Data curation, Investigation. **Matteo Calò:** Writing – original draft, Software, Methodology, Investigation, Data curation. **Gabriele Penello:** Project administration, Conceptualization. **Gabriel Yarce:** Writing – original draft, Investigation. **Walter Mittelbach:** Project administration, Funding acquisition, Conceptualization.

Declaration of competing interest

The authors declare that they have no known competing financial interests or personal relationships that could have appeared to influence the work reported in this paper.

Acknowledgments

This work has received funding from the European Union's H2020 program under Grant Agreement No. 101036656.

Data availability

Data will be made available on request.

References

[1] Jacob R, Hoffmann M, Weinand JM, Linßen J, Stolten D, Müller M. The future role of thermal energy storage in 100% renewable electricity systems. Renewable Sustainable Energy Transition 2023;4:100059. https://doi.org/10.1016/j.rset.2023.100059.

[2] Zhang Y, Wang R. Sorption thermal energy storage: Concept, process, applications and perspectives. Energy Storage Mater 2020;27:352–69. https://doi.org/10.1016/j.ensm.2020.02.024.

[3] Yan T, Zhang H. A critical review of salt hydrates as thermochemical sorption heat storage materials: Thermophysical properties and reaction kinetics. Sol Energy 2022;242:157–83. https://doi.org/10.1016/j.solener.2022.07.002.

[4] Hua W, Yan H, Zhang X, Xu X, Zhang L, Shi Y. Review of salt hydrates-based thermochemical adsorption thermal storage technologies. J Storage Mater 2022;56:106158. https://doi.org/10.1016/j.est.2022.106158.

[5] Mohapatra D, Nandanavanam J. Salt in matrix for thermochemical energy storage - a review. Mater Today Proc 2023;72:27–33. https://doi.org/10.1016/j.matpr.2022.05.453.

[6] Ferchaud CJ, Scherpenborg RAA, Zondag HA, De Boer R. Thermochemical Seasonal Solar Heat Storage in Salt Hydrates for Residential applications – Influence of the Water Vapor pressure on the Desorption Kinetics of MgSO4.7H2O. Energy Procedia 2014;57:2436–40. https://doi.org/10.1016/j.egypro.2014.10.252.

[7] Pathak AD, Nedea S, Van Duin ACT, Zondag H, Rindt C, Smeulders D. Reactive force field development for magnesium chloride hydrates and its application for seasonal heat storage. PCCP 2016;18:15838–47. https://doi.org/10.1039/C6CP02762H.

[8] Clark R-J, Gholamibozanjani G, Woods J, Kaur S, Odukomaiya A, Al-Hallaj S, et al. Experimental screening of salt hydrates for thermochemical energy storage for building heating application. J Storage Mater 2022;51:104415. https://doi.org/10.1016/j.est.2022.104415.

[9] Zeng Y, Clark R-J, Galazutdinova Y, Odukomaiya A, Al-Hallaj S, Farid M, et al. Open-cycle thermochemical energy storage for building space heating: Practical system configurations and effective energy density. Appl Energy 2024;376:124218. https://doi.org/10.1016/j.apenergy.2024.124218.

[10] Zhang Y, Palomba V, Frazzica A. Understanding the effect of materials, design criteria and operational parameters on the adsorption desalination performance – a review. Energ Conver Manage 2022;269:116072. https://doi.org/10.1016/j.enconman.2022.116072.

[11] Gbenou TRS, Wang K. Kinetic analysis of poly-aluminum sulfate hydrate for low-temperature thermochemical heat storage. Appl Therm Eng 2022;210:118317. https://doi.org/10.1016/j.applthermaleng.2022.118317.

[12] Palomba V, Frazzica A. Recent advancements in sorption technology for solar thermal energy storage applications. Sol Energy 2019;192:69–105. https://doi.org/10.1016/j.solener.2018.06.102.

[13] Michel B, Dufour N, Börtlein C, Zoude C, Prud'homme E, Gremillard L, et al. First experimental characterization of CaCl2 coated heat exchanger for thermochemical heat transformer applications in industrial waste heat recovery. Appl Therm Eng 2023;227:120400. https://doi.org/10.1016/j.applthermaleng.2023.120400.

[14] AL-Hasni S, Santori G. The cost of manufacturing adsorption chillers. Therm Sci Eng Prog 2023;39:101685. https://doi.org/10.1016/j.tsep.2023.101685.

[15] Humbert G, Sciacovelli A. Design of effective heat transfer structures for performance maximization of a closed thermochemical energy storage reactor through topology optimization. Appl Therm Eng 2024;239:122146. https://doi.org/10.1016/j.applthermaleng.2023.122146.

[16] Jabbari-Hichri A, Bennici S, Auroux A. CaCl2-containing composites as thermochemical heat storage materials. Sol Energy Mater Sol Cells 2017;172:177–85. https://doi.org/10.1016/j.solmat.2017.07.037.

[17] Bérut E, Bois L, Touloumet Q, Outin J, Ondarts M, Postole G, et al. Characterization of silica-PEG-CaCl2 composite sorbents in an open thermochemical heat storage reactor. J Storage Mater 2023;72:108632. https://doi.org/10.1016/j.est.2023.108632.

[18] Frazzica A, Brancato V, Caprì A, Cannilla C, Gordeeva LG, Aristov YI. Development of "salt in porous matrix" composites based on LiCl for sorption thermal energy storage. Energy 2020;208:118338. https://doi.org/10.1016/j.energy.2020.118338.

[19] Dino GE, Palomba V, Nowak E, Frazzica A. Experimental characterization of an innovative hybrid thermal-electric chiller for industrial cooling and refrigeration application. Appl Energy 2021;281:116098. https://doi.org/10.1016/j.apenergy.2020.116098.

[20] Bell IH, Wronski J, Quoilin S, Lemort V. Pure and Pseudo-pure Fluid Thermophysical Property Evaluation and the Open-Source Thermophysical Property Library CoolProp. Ind Eng Chem Res 2014;53:2498–508. https://doi.org/10.1021/ie4033999.

[21] Seiler J, Lanzerath F, Jansen C, Bardow A. Only a wet tube is a good tube: understanding capillary-assisted thin-film evaporation of water for adsorption chillers. Appl Therm Eng 2019;147:571–8. https://doi.org/10.1016/j.applthermaleng.2018.08.024.

[22] Lanzerath F, Seiler J, Erdogan M, Schreiber H, Steinhilber M, Bardow A. The impact of filling level resolved: Capillary-assisted evaporation of water for adsorption heat pumps. Appl Therm Eng 2016;102:513–9. https://doi.org/10.1016/j.applthermaleng.2016.03.052.

[23] Palomba V, Frazzica A. Experimental study of a fin-and-tube heat exchanger working as evaporator in subatmospheric conditions. Appl Therm Eng 2020;175:115336. https://doi.org/10.1016/j.applthermaleng.2020.115336.

[24] Thimmaiah PC, Sharafian A, Rouhani M, Huttema W, Bahrami M. Evaluation of low-pressure flooded evaporator performance for adsorption chillers. Energy 2017;122:144–58. https://doi.org/10.1016/j.energy.2017.01.085.

[25] Volmer R, Eckert J, Füldner G, Schnabel L. Evaporator development for adsorption heat transformation devices – Influencing factors on non-stationary evaporation with tube-fin heat exchangers at sub-atmospheric pressure. Renew Energy 2017;110:141–53. https://doi.org/10.1016/j.renene.2016.08.030.

[26] Mikhaeil M, Nowak S, Palomba V, Frazzica A, Gaderer M, Dawoud B. Experimental and analytical investigation of applying an asymmetric plate heat exchanger as an evaporator in a thermally driven adsorption appliance. Appl Therm Eng 2023;228:120525. https://doi.org/10.1016/j.applthermaleng.2023.120525.

[27] Toppi T, Villa T, Vasta S, Mittelbach W, Freni A. Testing of a Falling-Film Evaporator for Adsorption Chillers. Energies 2022;15:1709. https://doi.org/10.3390/en15051709.

[28] Pan QW, Liu L, Wang B, Xu J, Ge TS. Design and experimental study on a small-scale silica gel/water adsorption chiller with heat and mass recovery scheme for solar energy use. Sol Energy 2023;252:91–100. https://doi.org/10.1016/j.solener.2023.01.052.

[29] Bau U, Baumgärtner N, Seiler J, Lanzerath F, Kirches C, Bardow A. Optimal operation of adsorption chillers: first implementation and experimental evaluation of a nonlinear model-predictive-control strategy. Appl Therm Eng 2019;149:1503–21. https://doi.org/10.1016/j.applthermaleng.2018.07.078.

[30] Cotti M, Fischer H, Adan O, Huinink H. A scaling rule for power output of salt hydrate tablets for thermochemical energy storage. J Storage Mater 2024;87:111395. https://doi.org/10.1016/j.est.2024.111395.

[31] Pan Q, Peng J, Wang R. Experimental study of an adsorption chiller for extra low temperature waste heat utilization. Appl Therm Eng 2019;163:114341. https://doi.org/10.1016/j.applthermaleng.2019.114341.

[32] He F, Nagano K, Togawa J. Experimental study and development of a low-cost 1 kW adsorption chiller using composite adsorbent based on natural mesoporous material. Energy 2020;209:118365. https://doi.org/10.1016/j.energy.2020.118365.

[33] Patel J, Maiti S. Experimental investigation of a small-scale evacuated tube-based solar adsorption chiller with emphasis on improving the cycle time. Energ Conver Manage 2023;292:117421. https://doi.org/10.1016/j.enconman.2023.117421.

[34] Du S, Cui Z, Wang RZ, Wang H, Pan Q. Development and experimental study of a compact silica gel-water adsorption chiller for waste heat driven cooling in data centers. Energ Conver Manage 2024;300:117985. https://doi.org/10.1016/j.enconman.2023.117985.

[35] Semprini S, Asenbeck S, Kerskes H, Drück H. Experimental and numerical investigations of an adsorption water-zeolite heat storage for refrigeration applications. Energy Procedia 2017;135:513–21. https://doi.org/10.1016/j.egypro.2017.09.492.

[36] Schreiber H, Lanzerath F, Reinert C, Grüntgens C, Bardow A. Heat lost or stored: Experimental analysis of adsorption thermal energy storage. Appl Therm Eng 2016;106:981–91. https://doi.org/10.1016/j.applthermaleng.2016.06.058.

[37] Palomba V, Vasta S, Freni A. Experimental testing of AQSOA FAM Z02/water adsorption system for heat and cold storage. Appl Therm Eng 2017;124:967–74. https://doi.org/10.1016/j.applthermaleng.2017.06.085.

[38] Köll R, Van Helden W, Engel G, Wagner W, Dang B, Jänchen J, et al. An experimental investigation of a realistic-scale seasonal solar adsorption storage system for buildings. Sol Energy 2017;155:388–97. https://doi.org/10.1016/j.solener.2017.06.043.

[39] Yan T, Zhang H, Yu N, Li D, Pan QW. Performance of thermochemical adsorption heat storage system based on MnCl2-NH3 working pair. Energy 2022;239:122327. https://doi.org/10.1016/j.energy.2021.122327.

[40] Fopah-Lele A, Rohde C, Neumann K, Tietjen T, Rönnebeck T, N'Tsoukpoe KE, et al. Lab-scale experiment of a closed thermochemical heat storage system including honeycomb heat exchanger. Energy 2016;114:225–38. https://doi.org/10.1016/j.energy.2016.08.009.